PCCP



PAPER

View Article Online



Cite this: Phys. Chem. Chem. Phys., 2022, **24**, 16712

Exploration of phase diagram, structural and dynamic behavior of [HMG][FSI] mixtures with NaFSI across an extended composition range†

Karolina Biernacka, 📭 Faezeh Makhlooghiazad, 📭 Ivan Popov, bc Haijin Zhu, 📭 Jean-Noël Chotard, Dd Luke A. O'Dell, Da Alexei P. Sokolov, Dbc Jennifer M. Pringle oand Maria Forsyth **

Hexamethylguanidinium bis(fluorosulfonyl)imide ([HMG][FSI]) has recently been shown to be a promising solid state organic ionic plastic crystal with potential application in advanced alkali metal batteries. This study provides a detailed exploration of the structural and dynamic behavior of [HMG][FSI] mixtures with the sodium salt NaFSI across the whole composition range from 0 to 100 mol%. All mixtures are solids at room temperature. A combination of differential scanning calorimetry (DSC), synchrotron X-ray diffraction (SXRD) and multinuclear solid state NMR spectroscopy is employed to identify a partial phase diagram. The 25 mol% NaFSI/75 mol% [HMG][FSI] composition presents as the eutectic composition with the eutectic transition temperature at 44 °C. Both DSC and SXRD strongly support the formation of a new compound near 50 mol% NaFSI. Interestingly, the 53 mol% NaFSI [HMG][FSI] composition was consistently found to display features of a pure compound whereas the 50 mol% materials always showed a second phase. Many of the compositions examined showed unusual metastable behaviour. Moreover, the ion dynamics as determined by NMR, indicate that the Na⁺ and FSI⁻ anions are significantly more mobile than the HMG cation in the liquid state (including the metastable state) for these materials

Received 26th April 2022, Accepted 17th June 2022

DOI: 10.1039/d2cp01910h

rsc.li/pccp

Introduction

Organic ionic plastic crystals (OIPC) have been increasingly attracting attention as solid state electrolytes for a range of electrochemical devices. 1-4 This unique type of material has been found to be a promising candidate for solid state electrolytes for batteries, due to inherent advantages of safety (being non-flammable and non-volatile) and reduced leakage problems.⁵⁻⁸ These solid materials are characterized by longrange order, displaying at the same time short-range disorder, and have at least one solid-solid phase transition before the melting temperature which results in a more disordered solid

Given the extensive choice of cation/anion combinations, it is possible to adjust the phase behaviour of OIPCs which simultaneously will influence the ion dynamics and hence their performance as electrolyte materials. Despite extensive research, the ion conduction mechanisms in OIPCs and their mixtures are still not clear, although it is suggested that diffusion can be achieved through either vacancies in the lattice or extended defects i.e. dislocations, grain boundaries. 1,10 Furthermore, the effect of ion chemistry, size, shape etc. on OIPC material properties is still not fully understood and thus there are ongoing efforts to design and interrogate new OIPCs and their mixtures in order to better understand how to control

In order to use OIPCs for energy storage systems, e.g., for advanced Na or Li batteries, an additional salt needs to be introduced into the OIPC. Encouragingly, the addition of this

structure and is often accompanied by higher ion dynamics. The term "plastic" arises from this higher degree of mobility that facilitates deformation (i.e. plasticity) under an applied stress without fracture. Molecular plastic crystals were extensively reviewed by Timmermans who suggested a correlation between the small entropies of melting ($<20 \text{ J K}^{-1} \text{ mol}^{-1}$) and plastic behaviour that may arise from the rotational disorder of the molecules even while retaining their long-range order.⁹

^a ARC Centre of Excellence for Electromaterials Science (ACES). Institute for Frontier Materials (IFM), Deakin University, Geelong, Victoria 3216, Australia. E-mail: maria.forsyth@deakin.edu.au

^b Chemical Sciences Division, Oak Ridge National Laboratory, Oak Ridge, Tennessee 37831, USA

^c Department of Chemistry, University of Tennessee, Knoxville, Tennessee 37996,

^d Laboratoire de Réactivité et de Chimie des Solides (LRCS), CNRS UMR 7314, Université de Picardie Jules Verne, 80039 Amiens Cedex, France

[†] Electronic supplementary information (ESI) available: The design of dip-cell, DSC thermogram, SXRD and NMR spectra, See DOI: https://doi.org/10.1039/ d2cp01910h

second salt component usually increases the ionic conductivity of the material, although it can also lead to more complex phase behaviour where the precise conduction mechanism is not always evident. The presence of solid-solid phase transitions that occur in all plastic crystals can also impact conduction processes as a function of temperature. For example, phase transitions result in more disordered structures and creation of defects and vacancies (as a result of the onset of rotational and/ or translational motion), which provides an ideal environment for target ion motions. 11 Phase I, which is the most plastic and conductive phase, by definition occurs just below the melting point.

Most previous studies have focused on either neat OIPCs and their structural and physical properties, or mixtures with a Li salt for lithium-ion battery applications. 12-15 Only a few Na salt mixtures with OIPCs have been reported thus far as promising solid state electrolyte candidates for Na ion batteries (NIBs).8,16

Among the few studied OIPCs for NIB applications, only few have been evaluated in terms of their phase diagrams. 17-19 Phase diagrams can provide detailed information about phase behavior, melting and crystallization temperatures. It is particularly useful for OIPC mixtures, where deep understanding of their phase behavior enables understanding of the material's microstructure which has a strong influence on ion dynamics and electrochemical properties. Phase diagrams also help to determine the compositions and temperatures in which OIPCs can serve as useful electrolytes (either liquid or solid state) for electrochemical systems.8,20,21

The first phase diagram of a mixture of an OIPC with sodium salt was reported by Forsyth et al., 22 who studied N-methyl-N-ethylpyrrolidinium bis(trifluoromethanesulfonyl)amide [C2mpyr][TFSI] with NaTFSI. They found 15 mol% NaTFSI to be the eutectic composition and a 63 °C eutectic transition. Despite a promising high eutectic temperature (for solid state electrolytes at room temperature), the conductivity of these electrolytes was low. After that, the phase behaviour of mixtures of triisobutylmethylphosphonium bis(trifluoromethylsulfonyl)imide ([P1i444] [TFSI]) with different concentrations of NaTFSI were studied and resulted in a phase diagram with a eutectic transition at 36 °C. Electrochemical tests were performed for two chosen concentrations (25 and 75 mol% NaTFSI) however, only a short cycling period of 10 min was employed during symmetric cell cycling.8 The presence of a liquid phase across a wide range of NaFSI compositions (35-70 mol%) in the case of the [C2mpyr][FSI] OIPC prevented this material from being used as solid state electrolyte although it shows promising behaviour in the liquid state.^{21,23}

hexamethylguanidinium bis(fluorosulfonyl)imide ([HMG][FSI]) OIPC was recently reported and its properties discussed.24-26 [HMG][FSI] was investigated in the context of sodium batteries, where it was mixed with sodium bis(fluorosulfonyl)imide (NaFSI) salt to enhance the ionic conductivity. Indeed, NaFSI addition of only 5 mol% resulted in increased conductivity and interestingly the conductivity was observed to be higher during the heating cycle (from -40 °C) than during the cooling cycle, which is not typically observed

for OIPCs. This behavior was explained by creation of large number of grain boundaries at the lowest temperature (phase III), which persisted in phase II after the solid-solid phase transition from phase III to phase II. The effect of the phase III formation on the ion dynamics was also investigated by solidstate nuclear magnetic resonance spectroscopy, where preferential crystalline orientation was observed by sample rotation. Those studies also showed ion decoupling in the 5 mol% NaFSI mixture, where the [FSI] anions were diffusing almost two orders of magnitude faster than the [HMG]⁺ cation.²⁴

Higher concentrations of alkali metal salts are often considered more beneficial in an electrochemical context, and hence this study explores in more detail the structural and dynamic behavior of this unusual organic ionic plastic crystal [HMG][FSI] in mixtures with NaFSI across the whole composition range from 0 to 100 mol%, utilizing differential scanning calorimetry (DSC), synchrotron X-ray diffraction (SXRD), electrochemical impedance spectroscopy (EIS) and broadband dielectric spectroscopy (BDS), and solid-state nuclear magnetic resonance (NMR) spectroscopy.

Experimental

Synthesis of electrolyte materials

Neat OIPC hexamethylguanidinium bis(fluorosulfonyl)imide, [((CH₃)₂N)₃C][FSI], was synthesized following our previously reported procedure.²⁶ The materials in this work were synthesized in a glovebox under argon atmosphere, by directly mixing appropriate amounts of sodium bis(fluorosulfonyl)imide (NaFSI) and neat [HMG][FSI] in various molar ratios. The mixtures were dissolved in dry acetonitrile, which was removed by 48 h of high-vacuum drying on a Schlenk line (24 h at room temperature followed by 24 h at 50 °C). 27 As a result, solid state materials were prepared: x mol% NaFSI (100 - x) mol%[HMG][FSI]. NaFSI (>99.9%, CoorsTek US) and Acetonitrile (≥99.9%, Merck Milipore Australia) were purchased commercially and used as received. Prepared samples were typically 1 g and for selective compositions such as 25 mol% different amounts were prepared, up to 4 g. Experimental uncertainty in weighing was ± 0.00005 g.

Differential scanning calorimetry (DSC)

Thermal measurements were performed using a Netzsch DSC 214 Polyma with liquid N2 cooling and data were analysed with Proteus 70 software. All electrolytes were prepared in a glovebox under argon atmosphere. Samples were dried under vacuum after which the required mass (5-15 mg) was hermetically sealed in an Al pan. An empty Al pan was used as a reference. The cooling and heating rate was 10 °C min⁻¹. All samples were first cooled to −95 °C before heating up to 100 or 150 °C (various temperatures were used due to the concentration effects on thermal decomposition) and kept there for 30 min. For all materials at least three heating and cooling scans were performed in order to firstly remove thermal history and ensure reproducibility of the following cycles. For all samples second

and third heating/cooling scans were consistent, eliminating the possibility of further phase transitions. To determine the phase diagram, T_{onset} was used for solid-solid phase transitions and the eutectic transition, whereas $T_{\rm peak}$ was used for the melting transition in all samples. The first heating scan was used for the phase diagram due to the metastability observed for many samples (only glass transition was observed during second and third heating scan).

Conductivity measurements

The ionic conductivity was measured for the neat [HMG][FSI] and its mixtures with NaFSI by two complementary techniques: electrochemical impedance spectroscopy (EIS) and broadband dielectric spectroscopy (BDS). The latter instrument enabled significantly lower temperatures and the use of an alternative cell configuration, which then verifies accuracy of the obtained data. Conductivity values were reproducible, as confirmed after performing multiple heating and cooling scans of the samples.

EIS measurements were performed on a MTZ-35 impedance analyzer (Bio-Logic Science Instruments, France) equipped with a Eurotherm 2204 temperature controller and driven by MT-Lab software. A temperature range of 30–100 °C with 10 °C intervals was used for all experiments. The samples were equilibrated for 30 min at each temperature. The frequency range applied was from 1 MHz to 50 mHz. A locally made dip conductivity cell (a dip cell) which consists of two platinum electrodes protected by glass (Fig. S1, ESI†) was used to measure all the samples. Cell preparation was conducted inside a glovebox under an argon atmosphere. The conductivity cell was put into a specially designed brass block, which was heated using a cartridge heater connected to a Eurotherm 2204e temperature controller. Liquid nitrogen and vermiculite insulation was used for cooling of the dip cell. The conductivity measurements were repeated on duplicate samples.

Conductivity measurements in BDS experiments were performed using an Alpha-A analyzer from Novocontrol. Data were collected over the frequency range of 100 mHz to 1 MHz. A Quatro temperature controller (Novocontrol) was used for variable-temperature measurements. The temperature protocol used was as follows: two scans from -40 to 100 °C conducted twice, followed by two scans from 30-100 °C, with 10 °C intervals for heating cycles and 20 °C intervals for cooling. All samples were stabilized for 20 min at each temperature to an accuracy of within ± 0.2 °C. A conductivity cell with upper and lower electrodes separated by a cap assuring a fixed electrode distance of 0.4 mm and a diameter of 10.2 mm was used during the experiments. The electrolytes were placed between the electrodes and measured with a voltage amplitude of 0.1 V.

Synchrotron X-ray powder diffraction (XRD) for structure determination

Variable-temperature synchrotron X-ray powder diffraction (XRD) on neat [HMG][FSI] and its mixtures with NaFSI was performed at the Australian Synchrotron, powder diffraction beamline. For this experiment, the wavelength was set at 0.827 Å with a zero shift of $\pm 0.006^{\circ}$ using a Si(111)

double-crystal monochromator before data acquisition. The samples were packed and sealed in 0.3 mm borosilicate glass capillaries (product of Charles Supper Company, Natick, MA, USA) under argon atmosphere inside the glove box. The samples were then cooled using an Oxford Cryosystems cryostream, which can be heated with a Cyberstar hot-air blower to up to 80 K. The ramp rate of 2 °C min⁻¹ and equilibration time of 5 min were used for the measurements. An array of 16 MYTHEN ID microstrip silicon detectors with each module spanning about 5° in 2θ covered data collection over the angular range from 2 to 76°. The data were collected at temperatures chosen according to different phases of the plastic crystal based materials for 20 s at two detector settings. Pdviper software was used for merging the data collected from both detectors for each experiments and plotting, analyzing the results.

Solid-state nuclear magnetic resonance (NMR)

Solid-state NMR spectroscopy was undertaken using a Bruker Avance III 11.7 T wide-bore solid-state spectrometer (500 MHz ¹H frequency) equipped with a static 5 mm HX extended temperature range probe. Samples were packed into 5 mm glass tubes in an argon atmosphere glovebox. The Topspin software was used for recording and analyzing the spectra. Measurements were performed at temperatures ranging from -40 to 100 °C, with a minimum waiting period of 10 min for the sample to reach a stable temperature. A Hahn echo pulse sequence was used for 19F and single-pulse excitation was used for ¹H and ²³Na. Gaussian/Lorentzian functions (or a CSA line shape in the case of 19F) were used to fit the curves and to calculate the peak widths (full width at half-maximum, FWHM) of various components to study the mobility of ions. Experimental uncertainty during spectra deconvolution was estimated manually to be $\pm 1\%$.

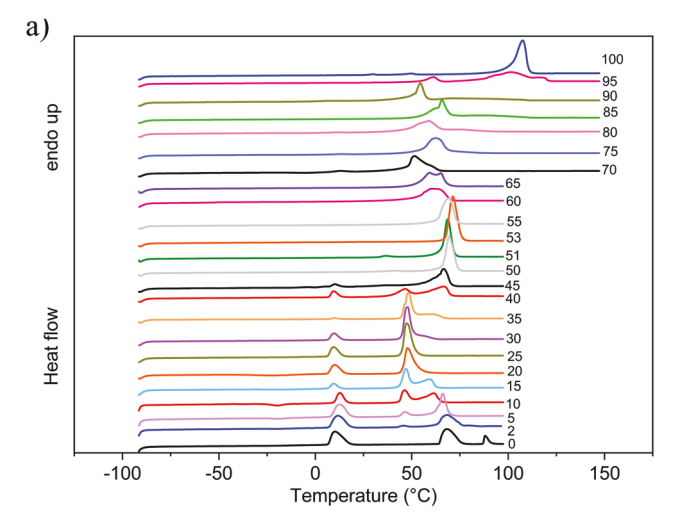
Pulsed-field gradient nuclear magnetic resonance (PFG-NMR)

¹H and ¹⁹F pulse-field gradient spin echo (PFG-SE) NMR was used for determination of the diffusivities of the [HMG]⁺ cation and [FSI] in [HMG][FSI] based electrolytes. The data was recorded every 10 °C from 20 to 100 °C temperature range and analyzed with Topspin. The measurement was performed on a Bruker Avance III 300 MHz spectrometer equipped with a Bruker diff50 probe. All samples were prepared inside an argonfilled glovebox. 23Na could not be used to measure the Na+ diffusion due to short relaxation times. Linewidth measurements described above are used for a qualitative assessment of Na⁺ mobility instead.

Results and discussion

Thermal phase behavior measured by differential scanning calorimetry

DSC heating traces for neat [HMG][FSI] and the series of mixtures with NaFSI are presented in Fig. 1. The neat OIPC is characterized by two solid-solid phase transitions (at 8 and 67 °C) followed



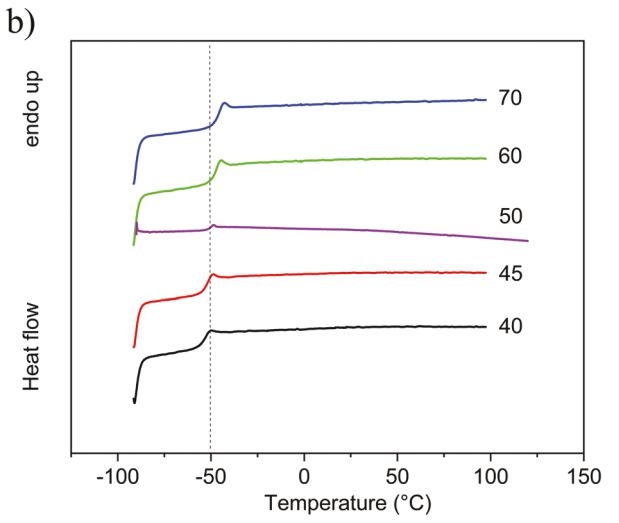


Fig. 1 (a) DSC thermograms of neat [HMG][FSI] (0), NaFSI (100) and their mixtures recorded on the first heating scan indicating phase transitions including solid-solid, eutectic and melting transitions. (b) Glass transition temperatures (T_{o}) of 40, 45, 50, 60 and 70 mol% NaFSI in [HMG][FSI] mixtures recorded during the second heating scan after melting and cooling the sample to -40 °C. All samples were measured at 10 °C min⁻¹.

by melting at 87 °C as previously reported. 25,26 As seen from Fig. 1a, the addition of the sodium salt to the OIPC significantly changes the thermal behavior of [HMG][FSI]. The mixture can be characterized by a broader, asymmetric melting transition which appears at lower temperatures than either the neat OIPC or the salt alone. This is because each substance acts as an impurity within the other. Moreover, after addition of 2 mol% NaFSI a new endothermic peak appears at 44 °C and the solidsolid phase transition merged with the melting temperature. This new peak grows with increasing Na salt concentration and reaches a maximum at 25 mol% NaFSI composition. At this concentration the peak is singular and sharp (in contrast to 20 or 30 mol% where a small shoulder was observed) suggesting that 44 °C is the eutectic temperature for this NaFSI/ [HMG][FSI] system and 25 mol% NaFSI in [HMG][FSI] is the eutectic composition. To confirm this hypothesis, the DSC

measurement was repeated using a slow scan rate of 2 °C min⁻¹ and the transition at 44 °C indeed gave a single, symmetric peak (Fig. S2, ESI†).

For the compositions below 50 mol%, several endothermic transitions were observed during the DSC experiments. These are assigned to solid-solid phase transitions, the eutectic transition and the final melt; the shape of the eutectic suggests that several phase transitions are close to the eutectic melt and hence overlap for some of the compositions. Nevertheless, the fact that the peak at 44 °C grows with increasing NaFSI until 25 mol% and then decreases again is further evidence for a eutectic transformation where above 44 $^{\circ}\mathrm{C}$ there is liquid phase and below there are two solid state phases co-existing.

Above 25 mol% NaFSI, a new melt appears which grows in intensity and shifts to higher temperatures, reaching a maximum at 53 mol%. The shape of the peak at this composition is again symmetric representing a congruent melt that can only happen if this is a single phase, new compound. We circle back to this composition again with synchrotron data discussed below, which supports this conclusion. With further increasing the NaFSI concentration above 50 mol%, the thermal phase behavior changed significantly - not only the disappearance of the solid-solid phase transition at 8 °C and the eutectic peak but also the melting peaks are characterized by a complex pattern, suggesting overlapping of different peaks. Unfortunately, even using a slow scan rate the separate peaks could not be resolved. It is suspected that this behavior that results in overlapping peaks might be arising from multiple phases existing in this system or nonuniform distribution of the two elements within the grains. A similar phenomenon termed 'segregation' is well known for metals and ceramics when concentration gradients are established across the grains.28 This can be eliminated by heat treatment, however for the high concentration of Na salt mixtures metastability was observed during the second DSC heating cycle, resulting in a supercooled liquid where a glass transition appeared at different temperatures depending on the NaFSI concentration. The glass transition peak shifted towards higher temperatures with increasing Na salt concentration, which can be seen in Fig. 1b. This trend was also seen previously for other OIPC/NaFSI mixtures. 23,29

By extracting the transition temperatures from the DSC thermograms, a partial phase diagram is presented in Fig. 2.

Due to the complex metastable phase behaviour for high NaFSI concentrations, we concentrate on compositions below 50 mol% NaFSI and an insert of DSC traces is presented on the right hand side of this phase diagram, as the exact determination remains a challenge. To determine the phase diagram, Tonset was used for the solid-solid phase transitions and eutectic transition, whereas T_{peak} was used for the melting transition in all samples.

Temperature dependent conductivity behaviour in OIPC mixtures

Ionic conductivities of the neat [HMG][FSI] and binary mixtures with various concentrations (5, 25, 45, 53, 55 and 70 mol%) of NaFSI were determined from EIS and BDS measurements.

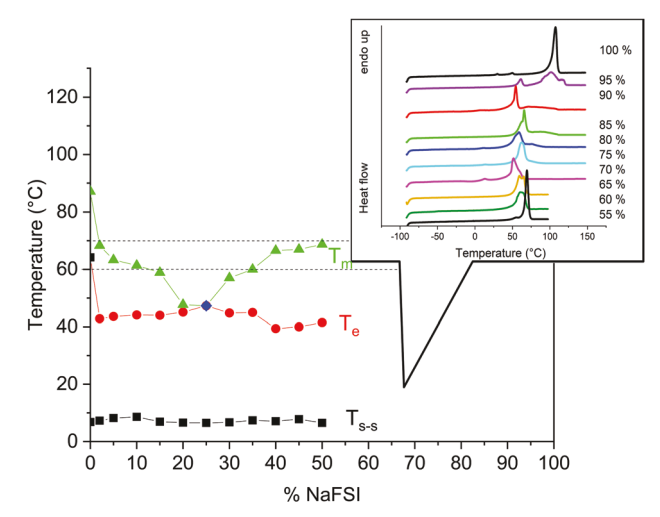


Fig. 2 Partial phase diagram for NaFSI in [HMG][FSI] binary electrolyte mixtures with insert of DSC traces for high Na salt concentrations. $T_{\rm e}$ refers to eutectic temperature, T_{s-s} solid-solid transition temperature and T_{m} melting temperature.

The temperature dependent ionic conductivity exhibits a general trend where all conductivity values increase steadily with increasing temperature, which can be seen from Fig. 3. The conductivity values presented in Fig. 3a were recorded by EIS (between 30 and 100 °C) and were collected during the second heating of the sample in order to have a consistent thermal history of the material and ensure good mechanical contact between the electrodes which is possible by melting and recrystallization of the samples. The issue with this measurement is that thermal history can have a very significant effect on phase the behaviour and conductivity, as seen from Fig. 3b and c, that were measured using BDS.

Conductivity behaviour for the neat OIPC and 5 mol% mixture is similar (Fig. 3a), showing a big conductivity increase passing through the solid-solid phase transition at 60 °C. On the other hand, for the eutectic composition at 25 mol% and higher NaFSI concentrations, no conductivity "jumps" were observed. Moreover, a decrease in conductivity with increasing concentration is observed. This conductivity dependence (Fig. 3a) is analogous to liquid electrolyte behaviour where conductivity gradually decreases with increasing Na salt concentration due to a higher viscosity of the liquid phase. This trend can be explained by metastability of the [HMG][FSI]/ NaFSI mixtures and the fact that the sample was cooled only to room temperature, which might be not sufficient to allow for full crystallization. Possibly [HMG][FSI] and 5 mol% NaFSI are less metastable in comparison to more concentrated systems, which could explain the observed solid state of neat OIPC and 5 mol% during the second heating scan.

The conductivity results were also confirmed by broadband dielectric spectroscopy (BDS). As can be seen from Fig. 3b and c, the ionic conductivity values are in agreement with the results obtained from EIS in the liquid phase, also shown in Fig. 3b along with the BDS data. Moreover, as expected, thermal history has a significant impact on the conductivity behavior. In

the case of 25 and 53 mol% NaFSI in [HMG][FSI] (Fig. 3b and c) cooling down to -40 °C resulted in different conductivity values than cooling down only to room temperature. This confirms the metastability, as mentioned before, and the fact that the sample is not fully crystallizing during cool down to 30 °C, which results in higher conductivity due to the presence of a mobile liquid fraction. This is due to the supercooling effect which significantly affects the material. After the sample has melted, and upon cooling again, the material requires time to fully crystallize again because of slow rearrangement of the ions. This means that the OIPC can be trapped in a metastable (high energy) state, resulting in either an amorphous solid or a trapped liquid state. Interestingly, hysteresis was previously observed for neat [HMG][FSI], where conductivity was higher on the heating scan than during cooling after melting, suggesting that, in the liquid state, the cation is relatively immobile in comparison to the anion, as explained in more detail in our previous publication.²⁴

The conductivity comparison presented in Fig. 3d. demonstrates a conductivity increase after the addition of NaFSI to neat [HMG][FSI] as would be expected based on previously reported OIPC electrolyte systems;²⁹⁻³¹ the conductivity of neat [HMG][FSI] is 4.2 \times 10^{-8} S cm $^{-1}$ at 40 $^{\circ}$ C, whereas after addition of 25 mol% NaFSI the conductivity increases by three orders of magnitude to $5.9 \times 10^{-5} \, \mathrm{S \ cm^{-1}}$ even in the solid state. Such a dramatic increase in conductivity suggests either an increase in defects, which supports increased ion dynamics, or the presence of an eutectic liquid phase. Noting that below 44 °C the system will be in the solid state, the conductivity does indeed suggest an increase in defects in this two-phase solid state material. A eutectic morphology can create more interfaces between alternating layers of two phases which are formed during the solidification process resulting in a socalled 'eutectic structure' which can be often very complex.²⁸ These interfaces can lead to extended defects and thus higher ion mobility. Increased defects and conductivity were previously reported for numerous OIPC-based composite electrolytes where significant interfacial disorded regions exist. 32-34

The effect of composition on phase behaviour studied by synchrotron XRD

Variable temperature Synchrotron X-Ray Powder Diffraction (SXRPD) experiments were performed for the neat [HMG][FSI], NaFSI, and mixtures of 25 mol%, 50 mol% and 53 mol% NaFSI in [HMG][FSI]. From the powder pattern comparison of all samples, it was confirmed that no pristine NaFSI could be found in any of the mixtures (Fig. S3, ESI†).

The 50 and 53 mol% NaFSI were chosen for the analysis here due to the somewhat unexpected DSC results that suggested that a new compound forms at the non-stoichiometric composition of 53 mol% NaFSI (50 mol% would have been the expected composition for a 1:1 compound). DSC measurements were repeated multiple times, and 50-53 mol% samples were synthesized multiple times, however 53 mol% was always characterized by sharp, congruent melting peak at the highest temperature among the 50, 51, 52 and 53 mol% mixtures.

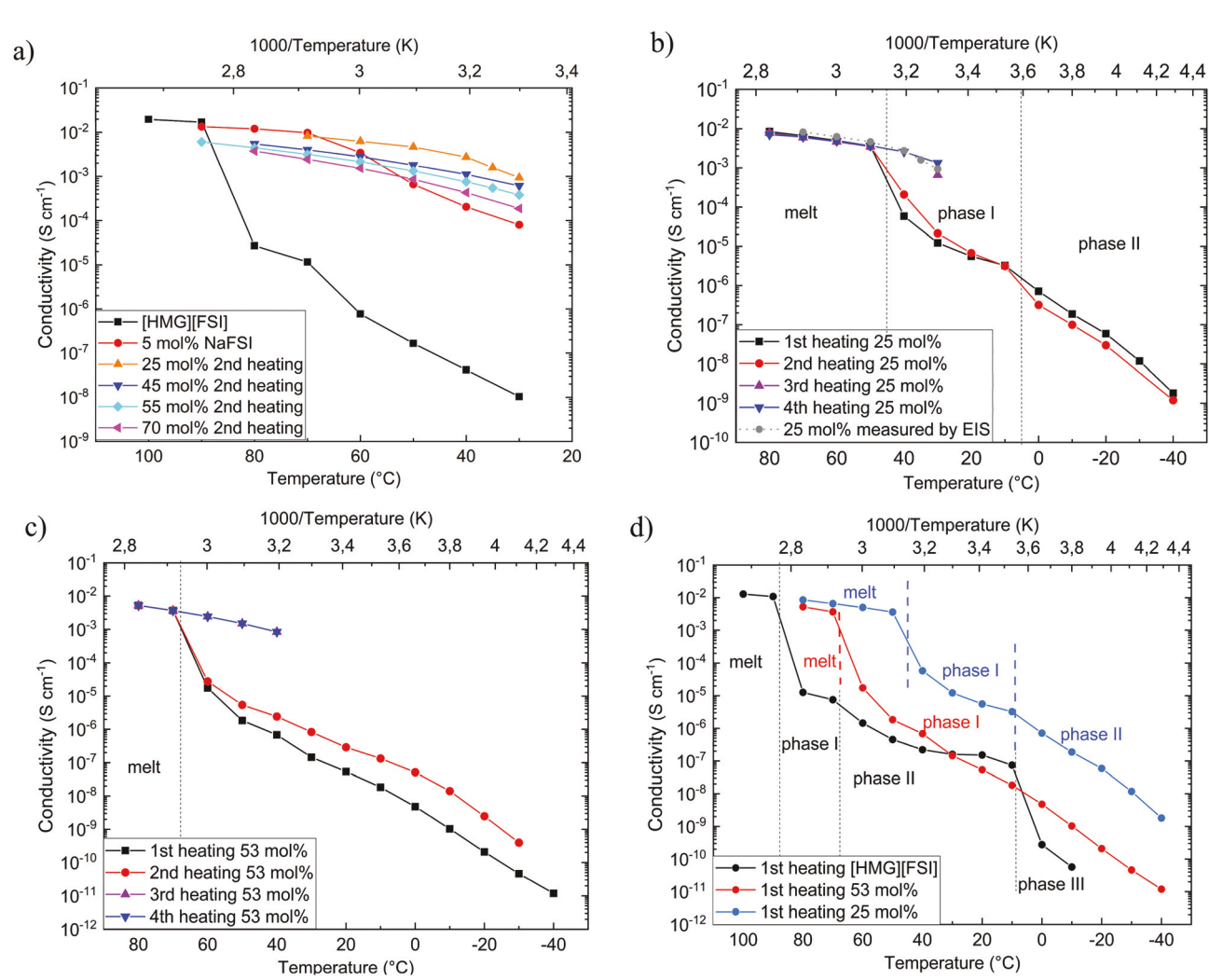


Fig. 3 (a) lonic conductivity of [HMG][FSI] electrolytes with various concentrations of NaFSI recorded during second heating measured by EIS. (b) 4 heating cycles of 25 mol% NaFSI with grey indicating EIS measurement (c) 53 mol% NaFSI electrolytes measured by BDS. (d) Comparison of 1st heating cycle of [HMG][FSI], 25 mol% and 53 mol% NaFSI measured by BDS. The dashed lines are indicating solid-solid and melting transitions determined by DSC. Each solid phase is labelled by Roman numerals.

We considered the possibility that an impurity exists in one or other of the starting materials which may give an 'offstoichiometry' compound but there was no evidence of this in the analysis.

The SXRPD analysis provides further confirmation that, at 53 mol% NaFSI, a new crystal structure arises that is different from neat [HMG][FSI] and also from the other mixtures. Moreover, from comparison of SXRPD patterns of 25, 50 and 53 mol% it can be seen that both the eutectic composition (25 mol% NaFSI - Fig. 4) and the 50 mol% samples (Fig. S4, ESI†) has diffraction peaks consistent with a mixture of the pure [HMG][FSI] OIPC and this new compound that is seen at 53 mol% NaFSI. The relative intensities of the observed phases suggest that the 25 mol% contains more neat [HMG][FSI] than the 50 mol%. However, for both the 25 mol% and 50 mol% NaFSI, some peaks were slightly shifted. This could be due to a solid solution mechanism between the cations (Na⁺ and [HMG]⁺) in the different structures. Moreover, some intensity

variabilities between these samples were observed. For example, some of the OIPC related peaks in 25 mol% NaFSI were much more intense than equivalent peaks from the pure [HMG][FSI]. This is especially true for low temperature phases and is likely related to preferential orientation which was also previously reported for [HMG][FSI].²⁴

With respect to temperature, all peaks shift towards lower angles with increasing temperature (Fig. S5, ESI†) due to an increase in unit cell parameters. This increase in *d* spacing has been previously observed for other OIPCs. Unfortunately, despite significant attempts, we have been unable to solve the crystal structure for the new compound and even defining satisfactory cell parameters remains a challenge.

Ion dynamics and structure using solid-state NMR spectroscopy

Variable temperature ²³Na, ¹H, ¹⁹F solid-state NMR was performed for the eutectic composition and 50 mol% NaFSI. Each

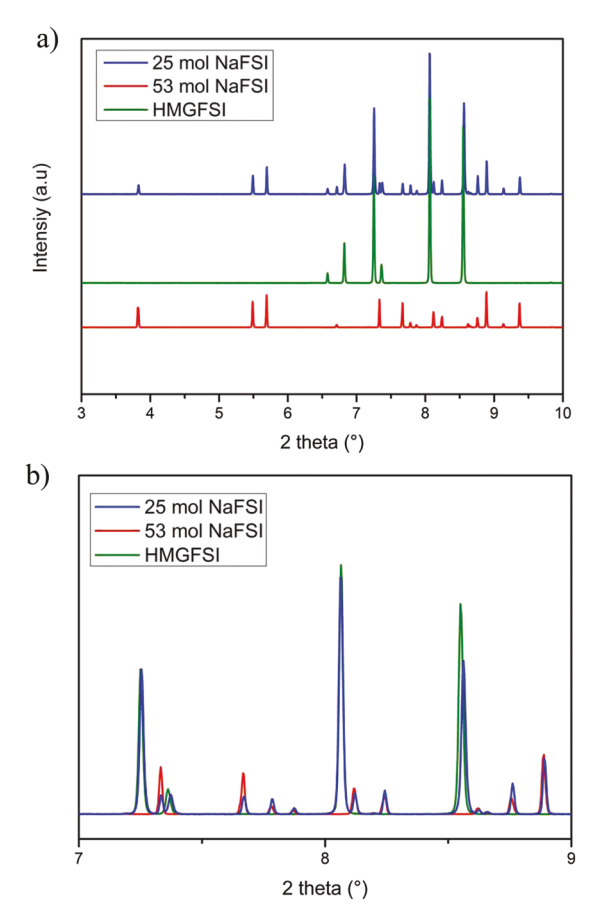
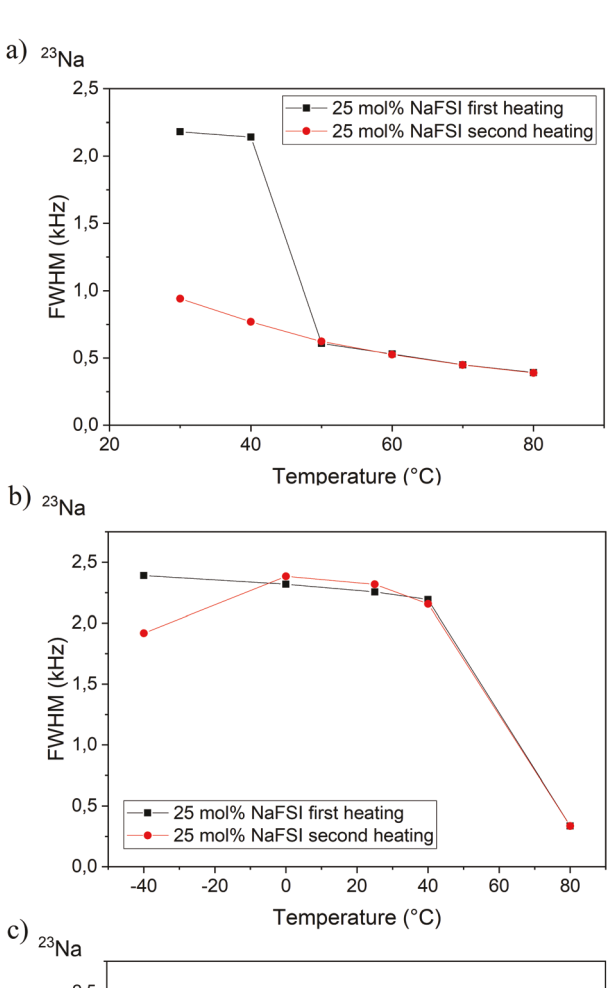


Fig. 4 Synchrotron X-Ray Powder Diffraction patterns measured at 25 °C of 25 mol% NaFSI (blue), 53 mol% NaFSI (red) and [HMG][FSI] (green) (a). The 25 mol% NaFSI pattern (blue) is the combination of [HMG][FSI] pattern (green) and 53 mol% NaFSI pattern (red) (b).

of the nuclei was used to study a different type of ion in the material: ¹H NMR was used to study the [HMG]⁺ cation, ¹⁹F for the [FSI]⁻ anions and ²³Na for the Na⁺ ions. The NMR peak full width at half maximum (FWHM) values for ²³Na and stackplots of NMR spectra of ¹⁹F, ¹H nuclei are presented in Fig. 5-7 respectively. In order to study the influence of metastability and thermal history on structural and dynamic behaviour of sodium doped [HMG][FSI], two heating cycles (as for BDS and XRD studies) were performed. The most significant changes are observed for ²³Na near 40 °C (close to the eutectic temperature of 44 °C) where a sudden narrowing occurs from 2.14 kHz to 0.77 kHz (Fig. 5a). For the [HMG]⁺ cation and [FSI]⁻ anion, more subtle changes are seen in the ion dynamics until 80 $^{\circ}\mathrm{C}$ where a very narrow, liquid like peak appears. For temperatures from zero to 40 °C a very minor narrow component appears on top of the broader component and the intensity of this component increases with increasing temperature as can be seen from Fig. 6 and 7. This minor component has previously been associated with diffusing ions and thus accounts for the increasing conductivity discussed above. Furthermore, the Na+ mobility (as determined from the FWHM linewidth for ²³Na) in the 25 mol% NaFSI sample recorded during two



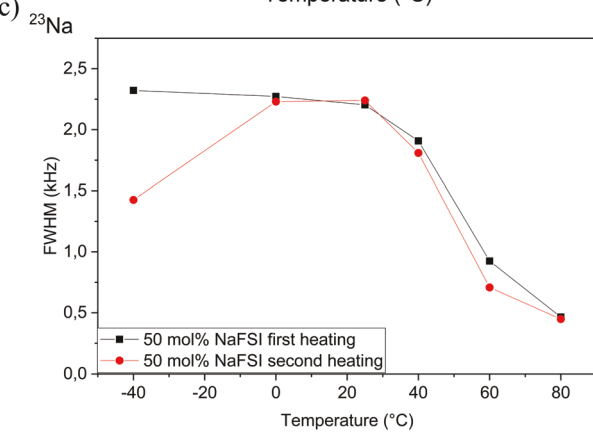


Fig. 5 Comparison of NMR peak full width half maxima (FWHM) of the ²³Na NMR spectra as a function of temperature for the eutectic composition (25 mol% NaFSI in [HMG][FSI]) during two heating cycles: from 30 to 80 $^{\circ}$ C (a) and from -40 to 80 $^{\circ}$ C (b) and 50 mol% NaFSI in [HMG][FSI] during two heating cycles: from -40 to 80 °C (c).

heating cycles from 30 to 80 °C is significantly higher at 30 °C during the second heating scan (Fig. 5a). In the case of static ions, a combination of second-order quadrupolar broadenings (reflecting the symmetry of the surrounding electronic environment) and chemical shift distributions (local structural disorder) are contributing to the 23Na NMR line width. Both of these contributions will undergo motional averaging due to ion dynamics, which will cause Na⁺ exchange between the various ion sites. Additionally, motion of **Paper**

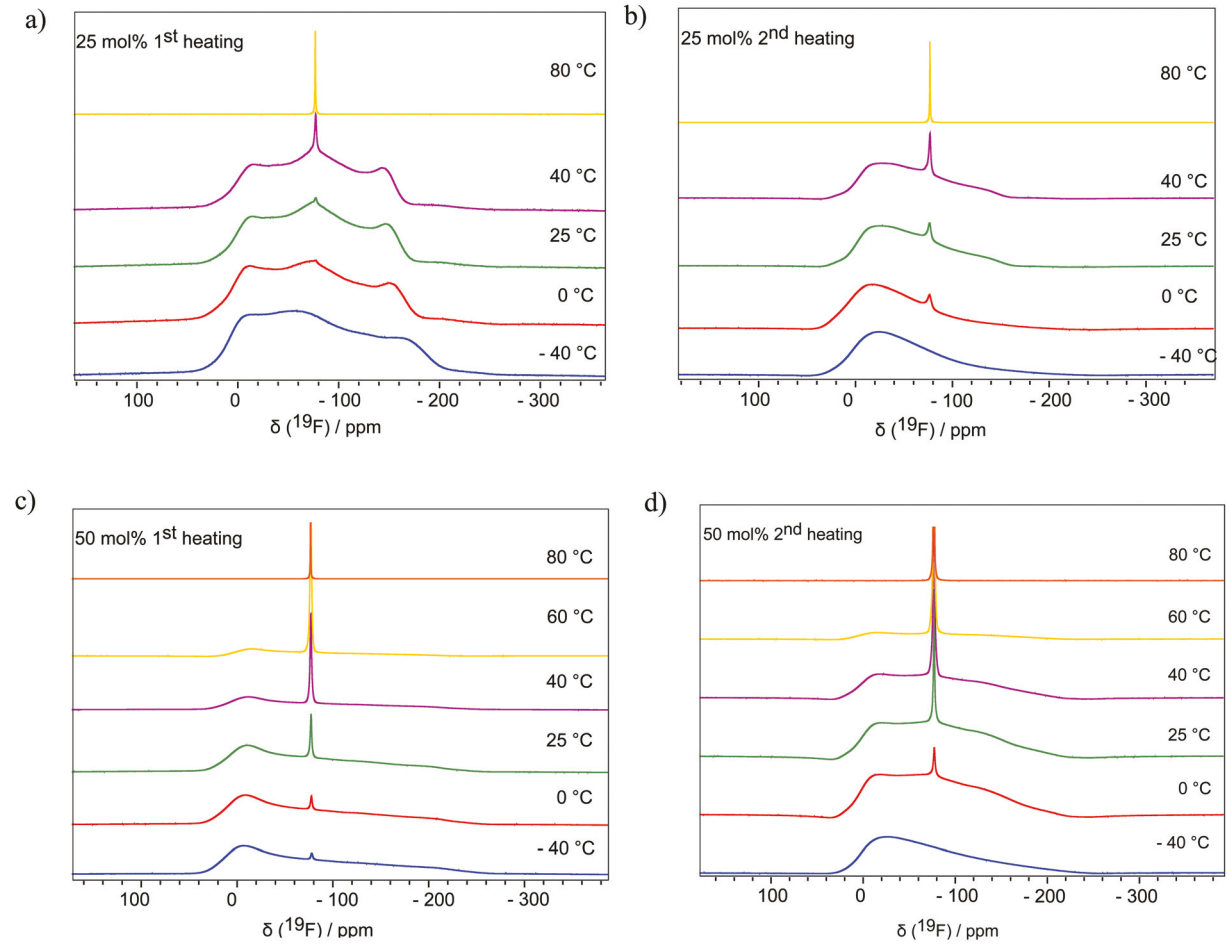


Fig. 6 19F spectra: stack spectra of 25 mol% NaFSI mixture recorded at various temperatures during the first (a) and second (b) heating scan from -40 to 80 °C and 50 mol% NaFSI mixture recorded during first (c), second (d) heating scan from -40 to 80 °C

the OIPC cations and anions surrounding the Na+ would have a similar effect, therefore in order to distinguish motion of Na⁺ from the motion of the surrounding ions, ¹H and ¹⁹F diffusion measurements were performed and discussed further below. Unfortunately, due to the rapid ²³Na relaxation, Na⁺ diffusivity could not be measured in any of the electrolytes. Significantly lower ²³Na FWHM values recorded during second heating scan are consistent with BDS measurements where cooling the sample to room temperature after melting followed by another measurement upon heating, resulted in a much higher conductivity.

From Fig. 5b and c we can see the 23Na peak FWHM comparison between two heating cycles performed from -40 to 80 °C for 25 mol% and 50 mol% NaFSI in [HMG][FSI], respectively. Cooling the materials down to -40 °C before reheating changes the behaviour, with the 23Na peak width being more consistent; i.e., both heating cycles show a wider line below 40 °C whose width decreases dramatically above the eutectic transition where the liquid phase appears. A comparison between Fig. 5a and b supports the thermal history dependent metastable behaviour in these materials, which is even more evident as we consider the 19F and 1H solid state NMR.

The two heating cycles were carried out from -40 to 80 $^{\circ}$ C to observe linewidth changes for 19F and 1H nuclei, as for the 23Na experiment. Changes in chemical shielding anisotropy (CSA) powder patterns during first and second heating cycle can be observed from Fig. 6a and b. None of the broad components could be accurately fitted with a single ideal CSA pattern, indicating the presence of some motional averaging or potentially multiple overlapping patterns from distinct fluorine environments. During the second heating scan, narrowing in CSA pattern is observed, which overall suggests increased dynamics (motional averaging of the CSA). The shape of the CSA (i.e., the asymmetry) in Fig. 6b suggests axial rotation of the anion.11

Interestingly, the ¹⁹F lineshape of 25 mol% NaFSI material that was recorded during the second heating scan (Fig. 6b) is similar to 19F lineshape recorded for 50 mol% electrolyte during both first and second heating cycles (Fig. 6c and d). As explained in the XRD section above, 25 mol% consists mostly of neat [HMG][FSI] and a small amount 53 mol% NaFSI (whose structure is very close to the 50 mol% NaFSI structure). Moreover, based on NMR and XRD data, 50 and 53 mol% mixtures seems to be less metastable and crystallize easier than

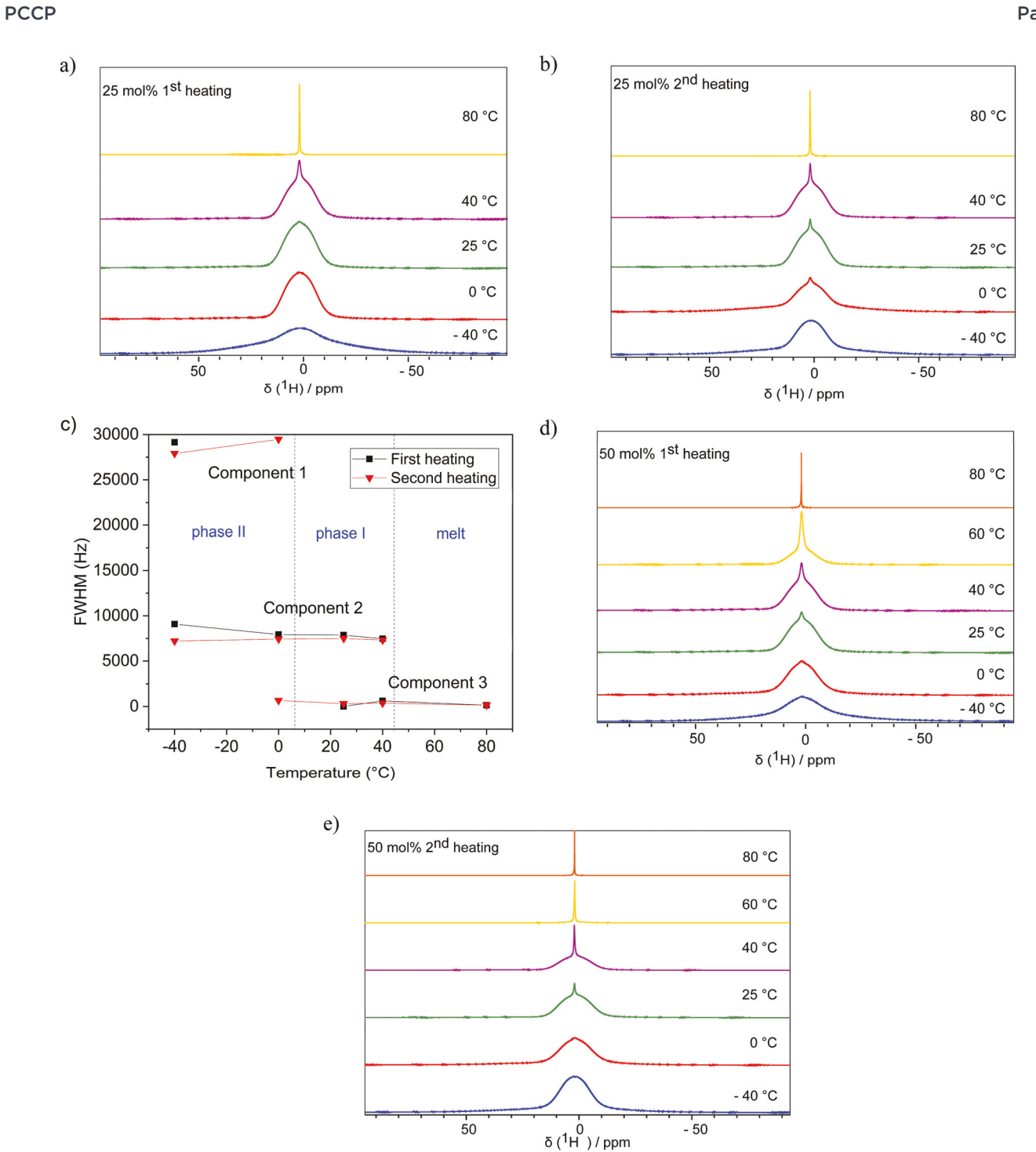


Fig. 7 The evolution of ¹H spectra versus temperature for 25 mol% NaFSI recorded during first (a) and second (b) heating scan -40 to 80 °C. Experimental NMR line widths as function of temperature for ¹H (c) during first (black) and second (red) heating scan. Component 1 refers to static, immobile cations without dynamics, component 2 with intermediate dynamics and component 3 represents fully isotropically rotating and diffusive species. The blue, dash lines represent different phases, as determined by DSC. The evolution of ¹H spectra versus temperature for 50 mol% NaFSI recorded during first (d) and second (e) heating scan -40 to 80 °C.

neat [HMG][FSI] which has highly metastable behaviour.²⁴ Therefore different CSA patterns observed during first and second heating cycle for 25 mol% can be explained by the fact that most of [FSI] ions in this materials are coming from neat, highly metastable [HMG][FSI], and the similar ¹⁹F lineshapes of 25 mol% during

second heating cycle to the ones for 50 mol% can be possibly explained by easier crystallization of 50 mol% NaFSI than the neat OIPC which are both present in 25 mol% NaFSI mixture.

¹H spectra revealed several components with different peak widths (Fig. 7a and b). After peak deconvolution, up to 3

components were observed for various temperatures (Fig. 7c and Fig. S7, ESI†). Component 1, the broadest part of the peak, is attributed to immobile [HMG]+ species, with linewidths ca. 30 kHz. As the result of motional narrowing, the intermediate component, component 2 (linewidths ca. 9-7 kHz) can be observed with increasing temperature, reflecting more dynamic cations. This narrowing is a result of motional averaging of nuclear dipole-dipole interactions, which could potentially be due to -CH₃ group rotations, rotation of the [HMG]⁺ or [FSI]⁻ movement. However, our diffusivity measurements (Fig. 8), appear to rule out diffusive [FSI] at this temperature. Therefore component 2 is suspected to be arising from [HMG]⁺ cation dynamics (-CH₃ group rotations and/or axial rotations of the cation as a whole). Upon further temperature increase, an additional narrower ¹H signal appears (component 3, with linewidths ca. 600-150 Hz). This narrow component 3 must arise from fully isotropically rotating cations, representing a mobile fraction of the sample and diffusive [HMG]+ which is further confirmed by PFG-NMR. The amount of the narrow component was greater during second heating scan vs first cycle and component 3 appeared at a lower temperature during the second heating scan (0 °C) compared with the first heating scan (25 °C), which is in agreement with the expected metastability of the sample.

Considering that the Na⁺ present in the 25 mol% sample comes only from the 53 mol% part of the mixture, the lack of difference in Na⁺ dynamics between the two heating cycles (Fig. 5b) is in agreement with other experiments where 53 mol% sample was shown to crystallize fully (XRD, BDS, NMR). Lower values of ²³Na FWHM were observed for 25 mol% which can be explained possibly by a difference in melting temperature for 25 mol% (44 °C) vs 50 mol% (53 °C) and the fact that 25 mol% is a combination of two phases, as discussed above, leading to more dynamics due to interfaces.

To compare the percentage of narrow NMR components (representing the mobile species) between the first and the second heating cycle, the integrations of the deconvoluted peaks were calculated. As discussed above, the area fractions

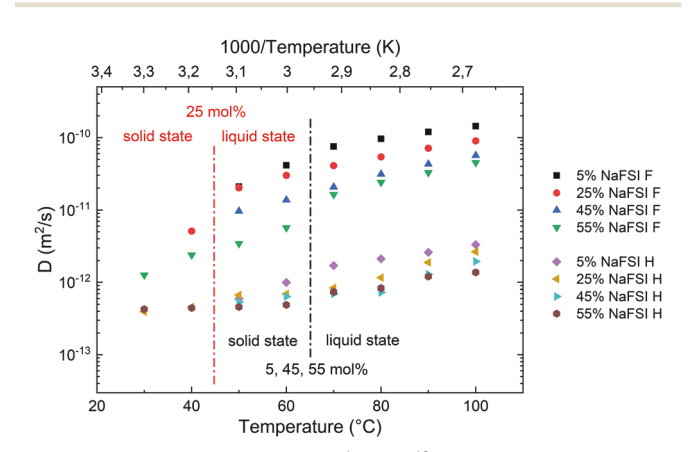


Fig. 8 Diffusion coefficients (D) of ¹H and ¹⁹F with different NaFSI concentrations in [HMG][FSI] measured by PFG NMR as a function of temperature

of the mobile component were greater during second heating cycle vs the first one. For example, for the 25 mol% sample at 40 °C the ¹H and ¹⁹F NMR spectra recorded during the first heating cycle both have 2% narrow component, slightly less than the second heating cycle, which were 3% (1H) and 4% (19F). A greater narrow component increase was observed for the 50 mol% sample, where initially 4% and 8% of mobile component was observed and these increased to 7% and 20% during the second heating cycle, for ¹H and ¹⁹F respectively. A noticeable increase in the narrow component fraction was observed for the 50 mol% sample with increasing temperature, after the solid-solid transition - for the ¹H spectra 7% at 40 °C was recorded during the second heating cycle, which increased to 22% at 60 °C during the first heating cycle and 100% during the second heating cycle, whereas the ¹⁹F spectra had 20% at 40 °C (second heating) which increased to 44% (first heating) and 59% (second heating) at 60 °C. Overall, the fraction of the mobile component was increasing with increasing temperature which is consistent with conductivity and PFG-NMR studies, where higher ion diffusion was recorded at higher temperatures.

The diffusivities of [FSI] and [HMG] in various binary mixtures (25, 45 and 55 mol% NaFSI in [HMG][FSI]) measured by pulsed field gradient nuclear magnetic resonance spectroscopy (PFG-NMR) can be seen in Fig. 8. These measurements are for diffusion of the various species in the liquid phase of the material. Unfortunately [FSI] and [HMG] diffusion in the neat OIPC, and for some of the measured samples at low temperatures, were not measurable due to the weak signals attributed to fast T_2 relaxation, as well as suspected slow diffusion. Moreover, Na+ diffusivity in all materials also could not be measured due to the rapid ²³Na relaxation.

From Fig. 8 it can be seen that temperature dependences of diffusivity are consistent with the ionic conductivity trends, where conductivity was decreasing with increasing concentration of NaFSI. Interestingly, across the entire studied temperature range, the anion diffusion coefficients are significantly higher than the proton diffusion coefficients. This trend was also observed for 5 mol% NaFSI in [HMG][FSI].24 As discussed in our previous work, it is suspected that ion decoupling observed in PFG-NMR studies may be caused by some selfassembly of [HMG]+ cations, even in the liquid phase, in a way that causes a much lower cation diffusivity compared to the [FSI] anions. In essence, the [HMG] cation provides a structuring but allows the anion (and presumably also the Na⁺ cation based on the narrow FWHM wideline values) to be more diffusive. Moreover, the difference between the diffusion of these ions becomes smaller at lower temperatures, as the [FSI] anion becomes less diffusive. [HMG]+ diffusivity values are relatively stable across the temperature range in contrast to the significant temperature dependence observed for [FSI]-. For example, for the 55 mol% sample, in the solid state (30 °C) the diffusion rates for [HMG]⁺ and [FSI]⁻ are $4.28 \times 10^{-13} \text{ m}^2 \text{ s}^{-1}$ and $1.26 \times 10^{-12} \text{ m}^2 \text{ s}^{-1}$ respectively, whereas at 100 °C (liquid state) they are $1.37 \times 10^{-12} \text{ m}^2 \text{ s}^{-1}$ and $4.5 \times 10^{-11} \text{ m}^2 \text{ s}^{-1}$. This may reflect a different diffusion mechanism in the solid

compared to the fully liquid state and also reinforces the concept that, in these mixtures, [HMG]+ retains a similar structuring in the liquid state as it has in the OIPC. Interestingly, this was not observed in related mixtures of [HMG][FSI] with lithium bis(fluorosulfonyl)imide (LiFSI), where the diffusivity values for the Li⁺, [HMG]⁺ and [FSI]⁻ were very similar in the 10 mol% LiFSI/LiTFSI and 90 mol% LiFSI/LiTFSI electrolytes.²⁵ The observations for the NaFSI mixtures may have positive implications for electrochemical behaviour in these mixtures even in liquid electrolytes and will be considered in our future work.

Conclusions

This work has demonstrated complex phase behaviour of [HMG][FSI] mixtures with NaFSI and resulted in a partial phase diagram where 25 mol% NaFSI was found to be a eutectic composition, and 44 °C the eutectic temperature. In addition, metastability observed during DSC experiments increased with increasing concentration of NaFSI in the electrolytes. Interestingly, during SXRPD analysis a new crystal structure of 53 mol% NaFSI was recorded which is different from neat [HMG][FSI] and from all other mixtures, confirming that 53 mol% NaFSI is a new compound. Moreover, the eutectic composition (25 mol% NaFSI) was found to show a combination of diffraction peaks of the pure [HMG][FSI] and this new compound 53 mol% NaFSI. This was also consistent with solid state NMR data, where ¹⁹F lineshapes of the 25 mol% sample recorded during the second heating scan appear to be similar to the ones for the 50 mol% sample.

Complex eutectic microstructure of 25 mol% NaFSI, which could be compared to composites, was characterized by increased defects and the highest conductivity of 5.9 \times 10⁻⁵ S cm⁻¹ (40 $^{\circ}$ C) of all investigated electrolytes (three orders of magnitude higher than the conductivity of the neat OIPC, 4.2×10^{-8} S cm⁻¹ at 40 °C). Moreover, ion decoupling was observed during PFG-NMR studies, across the whole temperature range. Anion diffusion coefficients were found to be significantly higher than the cation diffusion coefficients for all the investigated compositions. Interestingly, this behaviour was not observed for [HMG][FSI] mixtures with LiFSI or LiTFSI, suggesting positive implications for electrochemical properties of [HMG][FSI] based electrolyte for sodium batteries. Thus this study demonstrates the effect of sodium salt addition to [HMG][FSI] and the potential of these materials as solid state electrolytes for electrochemical devices.

Conflicts of interest

There are no conflicts to declare.

Acknowledgements

This work was financially supported by the Australian Research Council through the ARC Centre of Excellence for Electromaterials Science (grant no. CE140100012) and through the ARC Training Centre in Future Energy Storage Technologies IC180100049 (StorEnergy). An Australian Synchrotron beamtime allocation & SXRD beamline scientist (Dr Anita D'Angelo) are also acknowledged. The authors also wish to thank Dr Colin Kang (Deakin Univeristy, IFM) for assistance with the materials synthesis. The U.S. team acknowledges financial support from NSF Chemistry program (CHE-2102425 award).

Notes and references

- 1 J. M. Pringle, P. C. Howlett, D. R. MacFarlane and M. Forsyth, J. Mater. Chem., 2010, 20, 2056.
- 2 J. M. Pringle, Phys. Chem. Chem. Phys., 2013, 15, 1321-1716.
- 3 X. Pu, H. Wang, D. Zhao, H. Yang, X. Ai, S. Cao, Z. Chen and Y. Cao, Small, 2019, 15, 1-33.
- 4 X. Wang, R. Kerr, F. Chen, N. Goujon, J. M. Pringle, D. Mecerreyes, M. Forsyth and P. C. Howlett, Adv. Mater., 2020, 32, 1-21.
- 5 D. R. MacFarlane, M. Forsyth, P. C. Howlett, M. Kar, S. Passerini, J. M. Pringle, H. Ohno, M. Watanabe, F. Yan, W. Zheng, S. Zhang and J. Zhang, Nat. Rev. Mater., 2016, 1, 15005.
- 6 P. C. Howlett, J. Sunarso, Y. Shekibi, E. Wasser, L. Jin, D. R. MacFarlane and M. Forsyth, Solid State Ionics, 2011, 204-205, 73-79.
- 7 D. R. Macfarlane, J. Huang and M. Forsyth, Nature, 1999, 402, 792-794.
- 8 F. Makhlooghiazad, D. Gunzelmann, M. Hilder, D. R. MacFarlane, M. Armand, P. C. Howlett and M. Forsyth, Adv. Energy Mater., 2017, 7, DOI: 10.1002/aenm.201601272.
- 9 J. Timmermans, J. Phys. Chem. Solids, 1961, 18, 1-8.
- 10 J. Huang, A. Hill, M. Forsyth, D. MacFarlane and A. Hollenkamp, Solid State Ionics, 2006, 177, 2569-2573.
- 11 L. Jin, K. M. Nairn, C. D. Ling, H. Zhu, L. A. O'Dell, J. Li, F. Chen, A. F. Pavan, L. A. Madsen, P. C. Howlett, D. R. Macfarlane, M. Forsyth and J. M. Pringle, J. Phys. Chem. B, 2017, 121, 5439-5446.
- 12 Y. Zhou, X. Wang, H. Zhu, M. Yoshizawa-Fujita, Y. Miyachi, M. Armand, M. Forsyth, G. W. Greene, J. M. Pringle and P. C. Howlett, ChemSusChem, 2017, 10, 3135-3145.
- 13 M. Yoshizawa-Fujita, E. Kishi, M. Suematsu, T. Takekawa and M. Rikukawa, Chem. Lett., 2014, 43, 1909-1911.
- 14 Z. Bin Zhou and H. Matsumoto, Electrochem. Commun., 2007, 9, 1017-1022.
- 15 L. Jin, P. Howlett, J. Efthimiadis, M. Kar, D. MacFarlane and M. Forsyth, J. Mater. Chem., 2011, 21, 10171-10178.
- 16 F. Makhlooghiazad, M. Sharma, Z. Zhang, P. C. Howlett, M. Forsyth and L. F. Nazar, J. Phys. Chem. Lett., 2020, 11, 2092-2100.
- 17 M. Forsyth, T. Chimdi, A. Seeber, D. Gunzelmann and P. C. Howlett, J. Mater. Chem. A, 2014, 2, 3993-4003.
- 18 T. Chimdi, D. Gunzelmann, J. Vongsvivut and M. Forsyth, Solid State Ionics, 2015, 272, 74-83.
- 19 K. Matsumoto, R. Taniki, T. Nohira and R. Hagiwara, J. Electrochem. Soc., 2015, 162, A1409-A1414.

Paper

20 H. Yang, X. F. Luo, K. Matsumoto, J. K. Chang and R. Hagiwara, J. Power Sources, 2020, 470, 228406.

- 21 H. Yang, J. Hwang, Y. Wang, K. Matsumoto and R. Hagiwara, *J. Phys. Chem. C*, 2019, **123**, 22018–22026.
- 22 M. Forsyth, T. Chimdi, A. Seeber, D. Gunzelmann and P. C. Howlett, *J. Mater. Chem. A*, 2014, **2**, 3993–4003.
- 23 S. Malunavar, X. Wang, F. Makhlooghiazad, M. Armand, M. Galceran, P. C. Howlett and M. Forsyth, *J. Phys. Mater.*, 2021, 4, 044005, DOI: 10.1088/2515-7639/ac0800.
- 24 K. Biernacka, F. Makhlooghiazad, I. Popov, H. Zhu, J. N. Chotard, C. M. Forsyth, R. Yunis, L. A. O'Dell, A. P. Sokolov, J. M. Pringle and M. Forsyth, *J. Phys. Chem. C*, 2021, 125, 12518–12530.
- 25 K. Biernacka, D. Al-Masri, R. Yunis, H. Zhu, A. F. Hollenkamp and J. M. Pringle, *Electrochim. Acta*, 2020, **357**, 136863.
- 26 R. Yunis, A. F. Hollenkamp, C. Forsyth, C. M. Doherty, D. Al-Masri and J. M. Pringle, *Phys. Chem. Chem. Phys.*, 2019, 21, 12288–12300.
- 27 D. Al-Masri, R. Yunis, A. F. Hollenkamp and J. M. Pringle, Chem. Commun., 2018, 54, 3660–3663.

- 28 J. William, D. Callister and D. G. Rethwisch, *Materials Science and Engineering*, John Wiley Sons, Inc, 2014, vol. 9, pp. 266–267.
- 29 F. Makhlooghiazad, P. C. Howlett, X. Wang, M. Hilder, D. R. MacFarlane, M. Armand and M. Forsyth, *J. Mater. Chem. A*, 2017, 5, 5770–5780.
- 30 N. Iranipour, D. J. Gunzelmann, A. J. Seeber, J. Vongsvivut, A. F. Hollenkamp, M. Forsyth and P. C. Howlett, *J. Mater. Chem. A*, 2017, 5, 24909–24919.
- 31 L. Jin, P. C. Howlett, J. M. Pringle, J. Janikowski, M. Armand, D. R. MacFarlane and M. Forsyth, *Energy Environ. Sci.*, 2014, 7, 3352–3361.
- 32 X. Wang, H. Zhu, G. W. Greene, Y. Zhou, M. Yoshizawa-Fujita, Y. Miyachi, M. Armand, M. Forsyth, J. M. Pringle and P. C. Howlett, *Adv. Mater. Technol.*, 2017, 2, 1700046.
- 33 F. Nti, X. Wang and P. C. Howlett, *Mater. Adv.*, 2021, 1683–1694.
- 34 Y. Shekibi, S. J. Pas, N. M. Rocher, B. R. Clare, A. J. Hill, D. R. MacFarlane and M. Forsyth, *J. Mater. Chem.*, 2009, 19, 1635–1642.